Evaluating Stability of a Transient Cut during Endmilling using the Dynamic Cutting Force Model

Seokjae Kang*, Dong-Woo Cho** and Chong K. Chun*

* Department of Mechanical Engineering, Pohang University of Science and Technology, Pohang, Kyungbuk, South Korea

** Dept. of Mechanical Engineering Sun Moon University, Asan-si, ChoongNam, South Korea

ABSTRACT

Virtual computer numerical control (VCNC) arises from the concept that one can experience pseudo-real machining with a computer-numerically-controlled (CNC) machine before actually cutting an object. To achieve accurate VCNC, it is important to determine abnormal behavior, such as chatter, before cutting. Detecting chatter requires an understanding of the dynamic cutting force model. In general, the cutting process is a closed loop system that consists of structural and cutting dynamics. Machining instability, namely chatter, results from the interaction between these two dynamics. Several previous reports have predicted stability for a single path, using a simple cutting force model without tool runout and penetration effects. This study considers both tool runout and penetration effects, using experimental modal analysis, to obtain predictions that are more accurate. The machining stability during a corner cut, which is a typical transient cut, was assessed from an evaluation of the cutting configurations at the corner.

Keywords : Endmilling, transient cut, stability

1. Introduction

Machine tools are widely used in production and manufacturing and have significant roles in enhancing productivity. In order to maximize productivity, the speed at which the tools can machine, without causing deterioration in the system's stability, is crucial. Therefore, monitoring or evaluating machining stability is indispensable.

As the cutter rotates, the cutting configurations periodically change during endmilling; the uncut chip thickness changes continuously while the multi-point tool rotates and makes interrupted cuts. The dynamic cutting force model simulates the dynamic component of the cutting force by evaluating the relative displacement between that tool and workpiece that occurs from the vibrations caused by variation in chip thickness. Several studies have been reported in this field. An accurate static cutting force model was developed by treating the cutting coefficients as constants [1,2]. Budak and Altintas [3, 4, 5] predicted chatter through analytical estimation, and Hwang and Cho [6] proposed a model that considers the relative displacement between the tool and workpiece. Elbestawi [7] developed a dynamic model taking the damping between tool and workpiece into account, and Ismail [8] showed that more stable cutting is possible by giving some variation to the tool geometry. On the other hand, it was shown in [9] that the results for chatter prediction can differ according to the cutting force model used.

However, all of these models consider only the single path, whereas a transient cut, such as a corner cut, frequently occurs in real machining. Although one report

[10] mentions the possibility of chatter occurring during a corner cut, further research has not examined this matter.

In this study, the dynamic behavior of the tool was modeled through an experimental modal analysis, and the dynamic component was incorporated into the dynamic cutting force model. In addition, penetration and cutter runout effects were considered to permit a more accurate machining stability evaluation. The stability analysis during a transient cut was calculated using this model, and the effect of runout on the stability was investigated.

2. Structural dynamic modeling

The relative vibration from endmilling can be described as 2 DOF system using the concentrated mass model, as shown in Fig 1. The 2 DOF equation of motion for the relative amount of vibration during cutting can be described by equation (1).

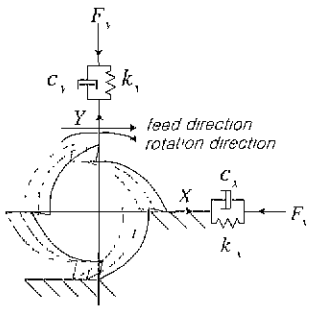

Fig. 1 Schematic diagram of tool vibration model

$$\begin{aligned} m_x\ddot{x} + c_x\dot{x} + k_x x &= F_x \\ m_y\ddot{y} + c_y\dot{y} + k_y y &= F_y \end{aligned} \tag{1}$$

These equations were numerically integrated to obtain the relative motion of the tool.

Dividing the left and right hand sides with modal mass, m_x, m_y, yields:

$$\begin{aligned} \ddot{x} + 2\zeta_x\omega_{nx}\dot{x} + \omega_{nx}^2 x &= \frac{F_x}{m_x} \\ \ddot{y} + 2\zeta_y\omega_{ny}\dot{y} + \omega_{ny}^2 y &= \frac{F_y}{m_y} \end{aligned} \tag{2}$$

The modal parameters were obtained through an experimental modal analysis; the results are shown in Table 1.

Table 1 Modal parameters of the tool.

	Mass (kg)	Freq. (Hz)	Damping ratio
X-axis	6.76	839	0.0314
Y-axis	6.62	861	0.0382

3. Cutting force modeling

3.1 Mechanistic cutting force model in endmilling [1]

An endmilling cutter can be divided into a finite number of disk elements. The total x-, y-, and z-force components acting on a flute at a particular instant are obtained from a numerical integration of the force components that act on an individual disk element. Summation over all of the flutes engaged in cutting yields the total force acting on the cutter at that instant in time.

Fig 2. shows schematic views of the endmilling process geometry and coordinate system adopted in this study. The angular position of the k-th axial disk element of the i-th flute, at the j-th angular position of the cutter, is given by Eqs. (3) and (4):

$$\theta(j) = -j\Delta\theta \tag{3}$$

$$\phi(i,j,k) = (i-1)\phi_c + (k\Delta a + \Delta a/2)\frac{\tan\theta_h}{R} + \theta(j) \tag{4}$$

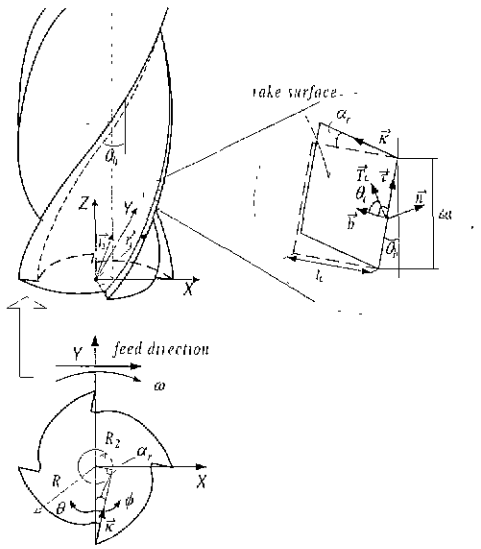

Fig. 2 Cutter geometry, coordinate system and unit vectors on the rake surface[1]

From the geometry shown in Fig 2.. the unit vectors on the rake face, $\vec{n}, \vec{\tau}, \vec{b}, \vec{\kappa}$, and the chip flow angle, $\vec{T}_c$, can be obtained. Then, the normal and frictional forces on the rake face, $dF_n(\phi)$ and $dF_f(\phi)$, can be calculated as from:

$$dF_n(\phi) = K_n T(\theta)\vec{n}(\alpha)dA_c \tag{5}$$

$$dF_f(\phi) = K_f K_n T(\theta)\vec{T}_c(\alpha)dA_c \tag{6}$$

where $dA_c = t_c(\phi)\cos\alpha_r(\Delta a/\cos\theta_h)$.

The three orthogonal components of the cutting forces can be determined at each disk element, in Cartesian coordinates, from the above equations. Summing them up for all of the disks along the tool axis, the following cutting forces are obtained:

$$\begin{aligned} F_x(j) &= \sum_k \sum_i F_x(i,j,k) \\ &= \sum_k \sum_i [A_1 K_n \cos(\phi - \alpha_r) + K_f K_n A_3 \cos\phi \\ &\quad - K_f K_n A_4 \sin(\phi - \alpha_r)] t_c(\phi) B_1 \end{aligned} \tag{7}$$

$$\begin{aligned} F_y(j) &= \sum_k \sum_i F_y(i,j,k) \\ &= \sum_k \sum_i [A_1 K_n \sin(\phi - \alpha_r) + K_f K_n A_3 \sin\phi \\ &\quad + K_f K_n A_4 \cos(\phi - \alpha_r)] t_c(\phi) B_1 \end{aligned} \tag{8}$$

$$\begin{aligned} F_z(j) &= \sum_k \sum_i F_z(i,j,k) \\ &= \sum_k \sum_i [-A_2 K_n + K_f K_n A_5] t_c(\phi) B_1 \end{aligned} \tag{9}$$

$$A_1 = \cos\theta_h / \sin\theta_{ik}$$

$$A_2 = (\sin\theta_h / \sin\theta_{ik}) \cdot \cos\alpha$$

$$A_3 = \sin\theta_h (\sin\theta_c - \cos\theta_c \cot\theta_{ik})$$

$$A_4 = \cos\theta_c / \sin\theta_{ik}$$

$$A_5 = \cos\theta_h (\sin\theta_c - \cos\theta_c \cot\theta_{ik})$$

$$B_1 = \cos\alpha_r \left(\frac{\Delta a}{\cos\theta_h} \right)$$

$$\cos\theta_{ik} = \vec{\tau} \cdot \vec{\kappa} = \sin\alpha_r \cdot \sin\theta_h$$

$$\sin\theta_{ik} = \sqrt{1 - \cos^2\theta_{ik}}$$

Cutting is performed over the range $\phi_{exit} < \phi < \phi_{entry}$ for each small disk element.

The range of angles over which the cutter is engaging with the workpiece, $\theta_{cutting}$, is:

$$\theta_{cutting} = \cos^{-1}\left(1 - \frac{d_w - (Y_a - Y_n)\cdot\sin\gamma - (X_a - X_n)\cdot\cos\gamma}{R}\right) \tag{10}$$

where γ is the angle the direction in which the tool is proceeding.

3.2 Direction of cutting considering the relative motion of the tool

The relative motion of a tool is usually neglected because its magnitude is very small compared to the cutting speed. However, in an unstable situation, such as chatter, the relative velocity of the tool becomes significant and thus cannot be ignored. This relative velocity may change the cutting direction of the individual disk elements, as is schematically shown in Fig 3. The amount that the cutting direction changes can be represented by the following equation:

$$\lambda = \left(\frac{V_r^r}{V_n + V_r^t}\right) \tag{11}$$

where V_r^r and V_t^t denote the relative velocity in the radial and tangential directions, respectively, which can be expressed as:

$$V_r^r = X_{rv} \cdot \sin\phi - Y_{rv} \cdot \cos\phi \tag{12}$$

$$V_t^t = -X_{rv} \cdot \cos\phi - Y_{rv} \cdot \sin\phi \tag{13}$$

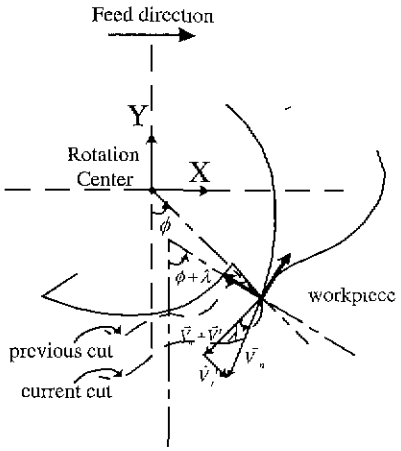

Fig. 3 Cutting direction that consider relative velocity of cutter

Therefore, when the relative motion between the tool and workpiece is considered, the actual cutting direction, which should be used in equations (7) - (9), is $\phi + \lambda$.

3.3 Model for the uncut chip thickness

Actual machining does not follow the nominal tool position exactly, for reasons such as the relative vibration and runout of the tool. Thus, the uncut chip thickness cannot be obtained only from the tool geometry, as described by

$$t_c = f_t \cdot \sin\phi \tag{14}$$

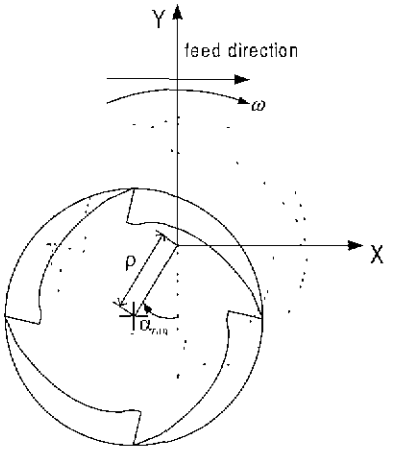

Fig. 4 Cutter runout offset and its location angle [2]

Taking the relative vibration and runout into account, the center position of the tool can be written as:

$$X_a(j,k) = X_n(j) + X_\rho(j) + X_{id}(j,k) \tag{15}$$

$$Y_a(j,k) = Y_n(j) + Y_\rho(j) + Y_{id}(j,k) \tag{16}$$

The nominal coordinates of the tool position, $X_n(j)$ and $Y_n(j)$, can be calculated from [1]

$$X_n(j) = X_n(j-1) + f_t \cos\gamma \cdot \frac{N_f}{360} \cdot \Delta\theta \tag{17}$$

$$Y_n(j) = Y_n(j-1) + f_t \sin\gamma \cdot \frac{N_f}{360} \cdot \Delta\theta \tag{18}$$

Tool runout, $X_\rho(j)$, $Y_\rho(j)$, can be determined from the runout offset and runout angle [1]:

$$X_\rho = -\rho \sin(\alpha_{run} - \theta(j)) \tag{19}$$

$$Y_\rho = -\rho \cos(\alpha_{run} - \theta(j)) \tag{20}$$

The tool-workpiece relative displacement in the x and y directions, $X_{rd}(j,k)$ and $Y_{rd}(j,k)$, can be obtained numerically in a similar way to that described in Section 2,

$$m_x X_{ra} + c_x X_{rv} + k_x X_{rd} = F_x \tag{21}$$

$$m_y Y_{ra} + c_y Y_{rv} + k_y Y_{rd} = F_y \tag{22}$$

To determine the uncut chip thickness, the equation of a line L_1 that connects the current tooth location and the center of the cutter (X_a, Y_a) was calculated. Circle equations C_1, C_2, C_3 and C_4 were used to describe the cutter at the previous three tooth locations as well as at the current one. The intersections between these circles and line L_1 were then calculated. The distances between these intersections and the current tooth location are possible uncut chip thicknesses. Of these distances, the smallest one was used as the uncut chip thickness in the dynamic cutting force model,

$$t_{cm}(i,j,k,m) = R - \sqrt{x_{tm}^2 + y_{tm}^2} \tag{23}$$

$$t_c = Max[0, Min(t_{cm}(i,j,k,m))] \tag{24}$$

t_{cm} Possible uncut chip thickness

(x_{tm}, y_{tm}) Location of the cutting edge in previous teeth

3.4 Determination of the cutting coefficients

Cutting coefficients can be considered as constants that depend upon the tool and workpiece materials [1]. This concept was adopted in this research.

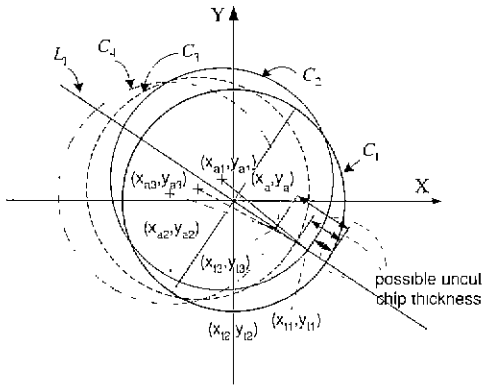

Fig. 5 Geometry for uncut chip thickness calculation

Measured cutting force signals were synchronized with one revolution of the simulated cutting forces that consider the angular position of the tooth. The variances of the cutting coefficients and chip flow angle were calculated at all of the combinations of runout offset, at increments of 0.001 mm, and runout angle, at increments of 1° . The runout parameters obtained at the minimum variance were selected and used with the cutting coefficients. One set of cutting coefficients was obtained with these parameters under cutting conditions of rpm = 1500, feedrate = 100 mm/min, radial depth = 10 mm, and axial depth = 8 mm. The results are listed in Table 2.

Table 2 Cutting coefficients and runout parameters

	K_f (N/mm^2)	θ_c $(rad.)$	ρ (mm)	α_{run} (deg.)
1140	0.9703	0.4358	0.011	172

4. Cutting process simulation

When a tool cuts in a straight line, the entry and exit cut are the only cases of transient cutting. However, transient cuts occur at most corners and cause the cutting configuration to change continuously. These ever-changing cutting configurations must be calculated to accurately predict cutting forces.

Cutting configurations during a corner cut are obtained by comparing the remaining portion of the cut from the previous tool path with that of the current tool path, as shown in Fig 6. There can be two cases as follows:

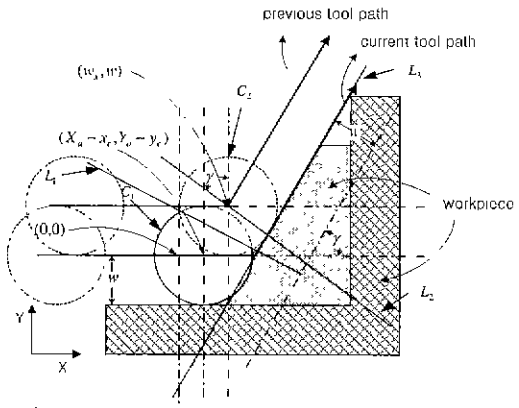

Fig. 6 Detailed schematic diagram at the cutting of corner

The intersection of circle C_1 and line L_1 occurs below the line L_2. The radial depth of cut d_w can be expressed by Equation (25), and calculated from the intersection of C_1 and L_1.

$$d_w = w + y_s \tag{25}$$

$$y_s = m_1(x_s - x_m) + y_m$$

$$x_s = \frac{-Q + \sqrt{Q^2 - 4P \cdot R}}{2P}$$

$$P = m_1^2 + 1$$

$$Q = 2(y_m \cdot m_1 - m_1^2 \cdot x_m - y_a \cdot m_1 - x_a)$$

$$R = m_1^2 \cdot x_m^2 + y_m^2 + y_a^2 + x_a^2 - R^2 - 2(m_1 \cdot x_m \cdot y_m + m_1 \cdot x_m \cdot y_a - y_m \cdot y_a)$$

$$m_1 = \frac{w_x - x_a}{y_a - w}$$

The intersection of circle C_1 and line L_1 occurs above line L_2. The radial depth of the cut d_w can be determined from Equation (26), and evaluated from the intersection of C_1 and L_3.

$$d_w = w + y_s \tag{26}$$

$$y_s = m_2(x_s - w_c) + n$$

$$x_s = \frac{-Q + \sqrt{Q^2 - 4P \cdot R}}{2P}$$

$$P = m_2^2 + 1$$

$$Q = 2(n \cdot m_2 - m_2^2 \cdot w_c - y_a \cdot m_2 - x_a)$$

$$R = m_2^2 \cdot w_c^2 + n^2 + y_a^2 + x_a^2 - R^2 - 2(m_2 \cdot w_c \cdot n + m_2 \cdot w_c \cdot y_a - n \cdot y_a)$$

$$m_2 = \tan(\gamma)$$

5. Experiments and results

5.1 Experimental procedure

Cutting forces were measured over a single line path and a corner cut for a vertical milling machine (ACE V30, Daewoo Heavy Industries). AL 2024-T6 workpieces were machined with a HSS flat endmill, with a diameter and overhang of 20 mm and 59.6 mm, respectively.

The corner was made before the corner cut experiment. The radial cut depth equaled the cutter radius, while the axial cut depth and rotation speed were varied. The prepared workpiece and the tool path are schematically shown in Fig 7.

Regions 1, 2, and 3 in Fig 7 are each 10 mm long. Regions 1 and 2 require transient cutting, because the cutter starts work on the corner, where the radial depth continuously changes. Regions 3 and 4 represent locations where the cutter changes direction by 90 degrees and disengages from the workpiece. At the boundary of region 3 and 4, slot cutting is performed instantaneously; thus, the cutting conditions rapidly change.

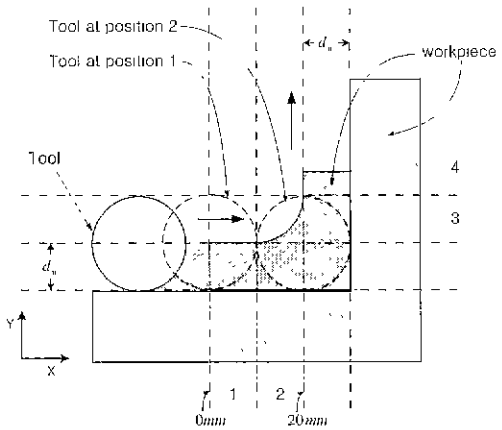

Fig. 7 Cutting experiment at the corner

The instant when the center of the tool enters region 1 was set as the origin of the coordinate system for all of the cutting experiments. The feed rate was 100 mm/min. Table 3 shows the cutting conditions used in the experiments. The cutting force signals were measured with a tool dynamometer (KISTLER 9257B) and a multi-channel charge amplifier (KISTLER 5019B), and were saved in a computer after passing through an A/D converter.

Table 3 Cutting conditions for each case

	Remark	depth of cut d_a (mm)	width of cut d_a (mm)	feed rate f_t (mm/min)	Spindle RPM (rev/min)
Case1	Corner	6	10 →20	100	1000
Case2	Straight	6	20	100	1000
Case3	Corner	5	10 →20	100	1000

5.2 Stability in the corner

Fig 8. and 9. show the measured cutting forces for CASE 1 and CASE 2, respectively. Fig 8. depicts the cutting forces for 200 cutter revolutions when chatter occurs at the corner. Fig 9. shows the cutting force for one cutter revolution during a single path cut. In CASE 1, at the instant the cutter finishes cutting in the X direction and changes its direction to the Y axis, the same cutting condition exists as in CASE 2. Chatter occurred at the corner momentarily, even under the same cutting conditions, whereas there was no chatter in the line path.

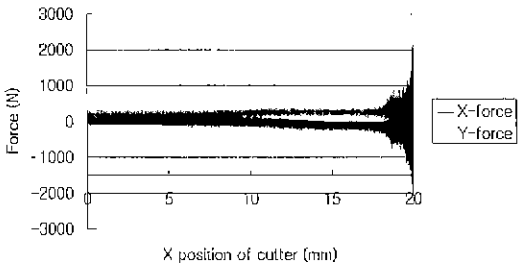

Fig. 8 Measured cutting force in the corner for CASE 1

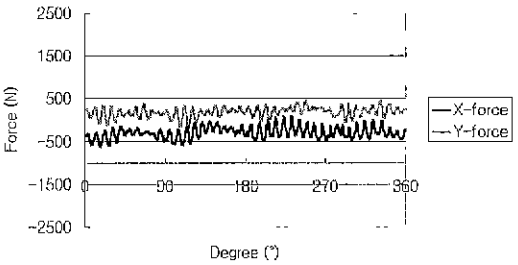

Fig. 9 Measured cutting force in the straight path for CASE 2

Fig 10. and 11. represent the simulated results for CASE 1 and CASE 2, respectively. The chatter observed in the experiments was also present in the simulations: chatter was noted at the corner and not in the straight path.

Fig 12. and 13. depict the results from the experiment and simulation, respectively. Both plots indicate that chatter occurs the instant the cutter enters the corner, and that the cutting regains its stability. In the figures, the cutter proceeded along the X-axis between 0 - 20 mm, and then changed direction and traveled along the Y-axis between 20 – 21 mm.

5.3 Effects of cutter runout on chatter

Fig 14. shows the simulated cutting force, under the same cutting conditions as in CASE 1, when cutter runout is not included in the model. This can be compared to Fig 10., where the forces were evaluated for CASE 1 and cutter runout was considered. The

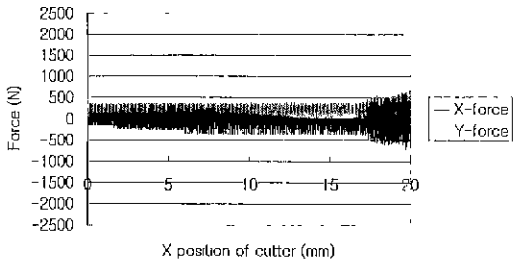

Fig. 10 Simulated cutting force in the corner for CASE 1

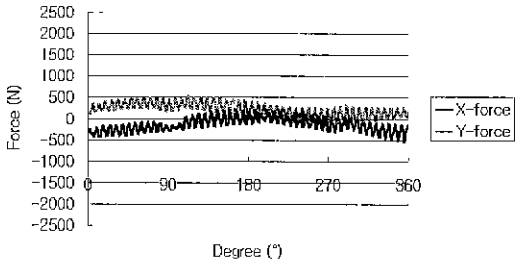

Fig. 11 Simulated cutting force in the straight path for CASE 2

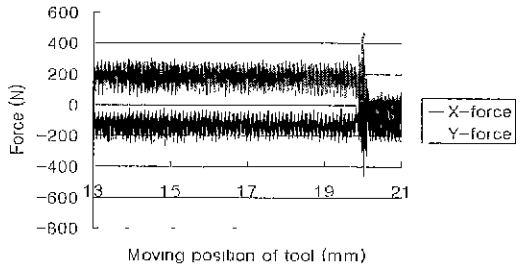

Fig. 12 Measured cutting force in the corner for CASE 3

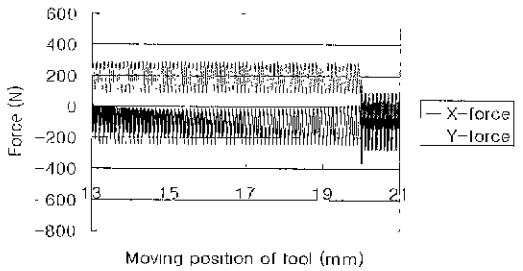

Fig. 13 Simulated cutting force in the corner for CASE 3

location of the tool when chatter began was 16.8 – 17 mm in Fig 10. and 16.3 - 16.4 mm in Fig 14. In the experiment, chatter was noted between 17.1 - 17.3 mm, as shown in Fig 8. Therefore, the cutter runout effect should be included in the dynamic cutting force model.

6. Conclusion

This paper investigated machining stability during a transient cut from endmilling. For the stability analysis, structural dynamics were evaluated for an endmill cutter, and a dynamic cutting force model was developed that included the effects of cutter runout. Comparisons were made between single path and corner cuttings for both experiments and simulations. Chatter is more likely to occur in a transient cut than in a single path cut. The model predicted the location of chatter onset more closely when the runout effect was considered.

Acknowledgements

The authors would like to thank the Science and Technology Policy Institute (STEPI) of Korea for supporting this work through the International Joint Project Research Fund (98-I-01-03-A-023).

References

1. W.S. Yun and D.W. Cho, "Determination of Constant 3D Cutting Force Coefficients and of Runout Parameters in End Milling," Transactions of NAMRI/SME, Vol. XXVII, pp. 87-92, 1999.
2. W.S. Yun, "A Study on the Cutting Force Model, Surface Error Analysis, and Cutting Process Simulation for a Virtual Machine Tool," Ph.D. thesis, POSTECH, 2000.
3. E. Budak and Y. Altintas, "Analytical Prediction of Chatter Stability in Milling-Part I: General Formulation," ASME J. of Dynamic Systems, Measurement, and Control, Vol. 120, pp. 22-30, 1998.
4. E. Budak and Y. Altintas, "Analytical Prediction of Chatter Stability in Milling-Part 2: General Formulation," ASME J. of Dynamic Systems, Measurement, and Control, Vol. 120, pp. 31-36, 1998.
5. Y. Altintas , S. Engin and E. Budak, "Analytical

Stability Prediction on and Design of Variable Pitch Cutter." ASME J. of Manufacturing Science and Engineering, Vol. 121, pp. 173-178, 1999

6. C.H.Hwang and D.W.Cho, "Chatter Prediction in Endmilling Using Dynamic Cutting Force Model," Journal of Korean Society of Precision Engineers, Vol. 16, No2, pp104-115, 1999.
7. M.A.Elbestawi, F.Ismail, R.Du and B.C.Ullagaddi, "Modelling Machining Dynamics Including Damping in the Tool-Workpiece interface," ASME Journal of Engineering for industry, Vol. 116, pp. 435-439, 1994.
8. F. Ismail and A. Bastami, "Improving Stability of Slender End Mills Against Chatter." Transactions of the ASME. Vol. 108, pp. 264-268, 1986.
9. Y. C. Shin and A. J. Waters, "A New Procedure to Determine Instantaneous Cutting Force Coefficient for Machining Force Prediction," Int. J. Mach. Tools Manufact., Vol. 37, pp. 1337-1351, 1997.
10. J. Tlusty, S. Smith and C. Zamudio, "New NC Routines for Quality in Milling," Annals of the CIRP Vol. 39, pp. 517-521, 1990.

NOMENCLATURE

m_x, m_y : Modal mass in the direction of the X and Y axes

c_x, c_y : Modal damping constant in the direction of the X and Y axes

k_x, k_y : Modal spring constant in the direction of the X and Y axes

$\theta(j)$: Cutter rotation angle

$\Delta\theta$: Cutter rotation angle increment

ϕ : Angular position of the cutting edge

ϕ_c : Flute spacing angle

i : Index of the flute

j : Index of cutter rotation

k : Index of the disk element

N_f : Number of the flute

θ_h : Helix angle

Δa : Height of the z-axis disk element

F_x, F_y, F_z : Cartesian coordinates of the cutting force components

K_n, K_f, θ_c : Cutting force coefficients: normal specific cutting force, frictional specific cutting force, and chip flow angle, respectively

ϕ_{entry} : Entry angle of the cutter

ϕ_{exit} : Exit angle of the cutter

$\theta_{cutting}$: Immersion angle of the cutter

R : Radius of the tool

t_c : Uncut chip thickness

f_t : Feed per tooth

α_r : Rake angle

(X_a, Y_a) : Actual position of the cutter center

(X_n, Y_n) : Nominal position of the cutter center

(X_ρ, Y_ρ) : Deviation caused by cutter runout

ρ, α_{run} : Radial runout offset for the cutter and its location angle

X_{ra}, X_{rv}, X_{rd} : Relative acceleration, velocity, and displacement of the tool in the direction of the X axis

Y_{ra}, Y_{rv}, Y_{rd} : Relative acceleration, velocity and displacement of the tool in the direction of the Y axis

d_d, d_w : Depth and width of cut, respective